RESEARCH OUTPUTS / RÉSULTATS DE RECHERCHE

Method for modeling additive color effect in photonic polycrystals with form anisotropic elements - the case of Entimus imperialis weevil

Mouchet, S.; Colomer, J.-F.; Vandenbem, C.; Deparis, Olivier; Vigneron, Jean-Pol

Link to publication

Download date: 21. May. 2019

Method for modeling additive color effect in photonic polycrystals with form anisotropic elements: the case of *Entimus imperialis* weevil

Sébastien Mouchet,* **Jean-François Colomer, Cédric Vandenbem, Olivier Deparis, and Jean-Pol Vigneron**

Department of Physics, University of Namur, rue de Bruxelles, 61, B-5000, Namur, Belgium

*sebastien.mouchet@unamur.be

Abstract: The calculation of the reflectance of photonic crystals having form-birefringent anisotropic elements in the crystal unit cell, such as cylinders, often turns out to be problematic, especially when the reflectance spectrum has to be computed according to different crystal orientations as in polycrystals for instance. The method we propose here solves this problem in the specific case of photonic crystals whose periodicities are such that there are no diffraction orders except Bragg reflection in the visible range. For a given crystal orientation, the crystal is sliced into layers and the periodic spatial variations of the dielectric function ε are homogenized. Thanks to that homogenization, the calculation can be performed using standard thin film computation codes. In order to demonstrate the usefulness of our method, we applied it to the case of a natural photonic polycrystal found on the cuticle of *Entimus imperialis* weevil which is a remarkable example of additive color effect. Although each photonic crystal grain of the polycrystal produces a single bright iridescent color, a non-iridescent green matt coloration is perceived by the human eye due to multiscale averaging effects.

References and links

1. J. D. Joannopoulos, S. G. Johnson, J. N. Winn, and R. D. Meade, *Photonic Crystals: Molding the Flow of Light* (Princeton University Press, Princeton, 2008).
2. S. John, "Strong Localization of Photons in Certain Disordered Dielectric Superlattices," Phys. Rev. Lett. **58,** 2486–2489 (1987).
3. E. Yablonovitch, "Inhibited Spontaneous Emission in Solid-State Physics and Electronics," Phys. Rev. Lett. **58,** 2059–2062 (1987).
4. O. Deparis and J.-P. Vigneron, "Modeling the photonic response of biological nanostructures using the concept of stratified medium: The case of a natural three-dimensional photonic crystal," Mater. Sci. Eng. B-Adv. **169,** 12–15 (2010).
5. M. G. Moharam and T. K. Gaylord, "Rigorous coupled-wave analysis of planar-grating diffraction," J. Opt. Soc. Am. **71,** 811–818 (1981).
6. J.-P. Vigneron and V. Lousse, "Variation of a photonic crystal color with the Miller indices of the exposed surface," in *Photonic Crystal Materials and Devices IV*, A. Adibi, S.-Y. Lin, and A. Scherer, eds., Proc. SPIE **6128,** 61281G (2006).

7. D. G. Stavenga, B. D. Wilts, H. L. Leertouwer, and T. Hariyama, "Polarized iridescence of the multilayered elytra of the Japanese jewel beetle, *Chrysochroa fulgidissima*," Philos. T. R. Soc. B **366,** 709–723 (2011).

8. P. Yeh, *Optical Waves in Layered Media* (Wiley-Interscience, Hoboken, 2005).

9. S. Mouchet, J.-P. Vigneron, J.-F. Colomer, C. Vandenbem, and O. Deparis, "Additive Photonic Colors in the Brazilian Diamond Weevil, *Entimus imperialis*," in *The Nature of Light: Light in Nature IV*, R. Liang, ed., Proc. SPIE **8480,** 848003 (2012).

10. S. Kinoshita, *Structural Colors in the Realm of Nature* (World Scientific Publishing Co, Singapore, 2008).

11. D. Van Opdenbosch, M. Johannes, X. Wu, H. Fabritius, and C. Zollfrank, "Fabrication of three-dimensional photonic crystals with tunable photonic properties by biotemplating," Photonics Nanostruct. **10,** 516–522 (2012).

12. R. A. Potyrailo, H. T. Ghiradella, A. Vertiatchikh, K. Dovidenko, J. R. Cournoyer, and E. Olson, "*Morpho* butterfly wing scales demonstrate highly selective vapour response," Nat. Photonics **1,** 123–128 (2007).

13. L. P. Biró, K. Kertész, Z. Vértesy, and Zs. Bálint, "Photonic nanoarchitectures occurring in butterfly scales as selective gas/vapor sensors," in *The Nature of Light: Light in Nature II*, Katherine Creath, ed., Proc. SPIE **7057,** 705706 (2008).

14. S. Mouchet, O. Deparis, and J.-P. Vigneron, "Unexplained high sensitivity of the reflectance of porous natural photonic structures to the presence of gases and vapours in the atmosphere," in *Nanophotonics IV*, D. L. Andrews, J.-M. Nunzi, and A. Ostendorf, eds., Proc. SPIE **8424,** 842425 (2012).

15. F. Song, H. Su, J. Han, D. Zhang, and Z. Chen, "Fabrication and good ethanol sensing of biomorphic SnO_2 with architecture hierarchy of butterfly wings," Nanotechnology **20,** 495502 (2009).

16. A. D. Pris, Y. Utturkar, C. Surman, W. G. Morris, A. Vert, S. Zalyubovskiy, T. Deng, H. T. Ghiradella, and R. A. Potyrailo, "Towards high-speed imaging of infrared photons with bio-inspired nanoarchitectures," Nat. Photonics **6,** 195–200 (2012).

17. X. Zang, Y. Tan, Z.Lv, J. Gu, and D. Zhang, "Moth wing scales as optical pH sensors," Sensor. Actuat B-Chem. **166-167,** 824–828 (2012).

18. B. D. Wilts, K. Michielsen, J. Kuipers, H. De Raedt, and D. G. Stavenga, "Brilliant camouflage: photonic crystals in the diamond weevil, *Entimus imperialis*," P. Roy. Soc. B-Biol. Sci. **279,** 2524–2530 (2012).

19. S. Vignolini, P. J. Rudall, A. V. Rowland, A. Reed, E. Moyroud, R. B. Faden, J. J. Baumberg, B. J. Glover, and U. Steiner, "Pointillist structural color in *Pollia* fruit," P. Natl Acad. Sci. USA **109,** 15712–15715 (2012).

20. J.-F. Colomer, P. Simonis, A. Bay, P. Cloetens, H. Suhonen, M. Rassart, C. Vandenbem, and J.-P. Vigneron, "Photonic polycrystal in the greenish-white scales of the African longhorn beetle *Prosopocera lactator* (Cerambycidae)," Phys. Rev. E **85,** 011907 (2012).

21. P. Simonis and J.-P. Vigneron, "Structural color produced by a three-dimensional photonic polycrystal in the scales of a longhorn beetle: *Pseudomyagrus waterhousei* (Coleoptera: Cerambicidae)," Phys. Rev. E **83,** 011908 (2011).

22. V. L. Welch, V. Lousse, O. Deparis, A. R. Parker, and J.-P. Vigneron, "Orange reflection from a three-dimensional photonic crystal in the scales of the weevil *Pachyrrhynchus congestus pavonius* (Curculionidae)," Phys. Rev. E **75,** 041919 (2007).

23. A. R. Parker, V. L. Welch, D. Driver, and N. Martini, "Opal analogue discovered in a weevil," Nature (London) **426,** 786–787 (2003).

24. M. Rassart, J.-F. Colomer, T. Tabarrant, and J.-P. Vigneron, "Diffractive hygrochromic effect in the cuticle of the hercules beetle *Dynastes hercules*," New J. Phys. **10,** 033014 (2008).

25. I. B. J. Sollas, "On the Identification of Chitin by Its Physical Constants," P. Roy. Soc. B-Biol. Sci. **79,** 474–481 (1907).

26. B. D. Wilts, K. Michielsen, H. De Raedt, and D. G. Stavenga, "Hemispherical Brillouin zone imaging of a diamond-type biological photonic crystal," J. Roy. Soc. Interface **9,** 1609–1614 (2012).

27. J.-P. Vigneron, M. Ouedraogo, J.-F. Colomer, and M. Rassart, "Spectral sideband produced by a hemispherical concave multilayer on the African shield-bug *Calidea panaethiopica* (Scutelleridae)," Phys. Rev. E **79,** 021907 (2009).

28. O. Deparis, C. Vandenbem, M. Rassart, V. L. Welch, and J.-P. Vigneron, "Color-selecting reflectors inspired from biological periodic multilayer structures," Opt. Express **14,** 3547–3555 (2006).

29. C. Pouya, D. G. Stavenga, and P. Vukusic, "Discovery of ordered and quasi-ordered photonic crystal structures in the scales of the beetle *Eupholus magnificus*," Opt. Express **19,** 11355–11364 (2011).

30. K. Kertész, Zs. Bálint, Z. Vértesy, G. I. Márk, V. Lousse, J.-P. Vigneron, M. Rassart, and L. P. Biró, "Gleaming and dull surface textures from photonic-crystal-type nanostructures in the butterfly *Cyanophrys remus*," Phys. Rev. E **74,** 021922 (2006).

1. Introduction

Photonic crystals (PCs) are among the most remarkable ordered optical materials. A PC is a periodic optical medium, consisting of regular spatial arrangements of materials with different refractive indices [1–3]. A 2D or 3D PC film has a finite thickness and periodic variations of the

dielectric permittivity, both in the direction perpendicular to the film surface and in the lateral directions, generaly giving rise to specular reflection and diffraction. This kind of material can be classified into the more general family of stratified media with lateral periodicity [4].

Usually, the optical reflectance, transmittance and absorbance of PC films can be calculated by plane wave methods such as the Rigorous Coupled Wave Analysis (RCWA) method [5, 6]. Details about RCWA can be found in Appendix A. This method relies on the calculation of the Fourier transform of the laterally periodic dielectric function $\varepsilon(\overrightarrow{r})$ and of the fields $\overrightarrow{E}(\overrightarrow{r})$ and $\overrightarrow{H}(\overrightarrow{r})$. As far as analytical treatment of the Fourier transform of $\varepsilon(\overrightarrow{r})$ is desired, the use of simple island shapes (cylinders or parallelepipeds with axes perpendicular to the layer interfaces) inserted in the layer host materials is required. Numerical calculations are usually rather demanding in computation time and convergence must be checked according to the number of plane waves. However, reflectance, transmittance or absorbance spectrum of periodic multilayer films (i.e. 1D PCs), which are periodic stacks of laterally homogeneous layers, can be computed by standard thin film solvers relying on a 1D scattering matrix (1D SM) formalism [7, 8]. In this case, Maxwell's equations are solved for stratified media only composed of homogeneous layers. The invariance of dielectric function $\varepsilon(\overrightarrow{r})$ in lateral directions leads to much shorter calculation times.

The calculation of the reflectance (or transmittance) for different crystal orientations of a PC film is much more complicated to perform when the crystal unit cell contains elements with form-birefringent anisotropy such as cylinders [9]. Crystal orientations, defined by Miller indices, are fictitious lines linking the PC nodes. Since some orientations can exhibit a higher density of nodes than others, the reflectance of the PC is different according to the orientation under which it is viewed. In order to solve this issue, we developed an approximation method allowing to calculate the reflectance of PC films with form anisotropic elements viewed under different orientations. Moreover, multiscale effects of specific structures, such as additive colors, were taken into account by calculating the reflectance of PC films according to different crystal orientations and incidence angles.

Hereafter, the calculation method is described first. Then the usefulness of our method is illustrated in the case of 3D PC grains (forming a polycrystal) found on the cuticle of the Brazilian weevil *Entimus imperialis* (Forster 1771). It is one nice example of structurally colored nanostructures found in living organisms [10]. In the case of insects, natural PCs consist of porous biopolymers such as chitin. Like many biological structures, the PC grains of the weevil were recently replicated by biotemplating [11]. Replicated structures can serve in biological applications such as gas, temperature or pH sensors [12–17]. The photonic structure of *Entimus imperialis*, also called diamond weevil, is formed by one single type of PC with different orientations [9, 18]. This multiscale aspect of the polycrystalline structure alters light propagation and gives rise to non-iridescent additive photonic coloration [9, 18, 19], which results from the spatial average of individual bright colors produced by each PC grain. Iridescent materials have colors which change according to the incident and viewing angles. The approach we used to model *Entimus imperialis* polycrystal took into account structural disorder and allowed us to explain why individual grains displayed bright colors whereas non-iridescent green coloration was observed in the far-field.

2. Calculation method

In order to model the multiscale optical properties of a photonic polycrystal resulting from specific orientations of the same crystal, we treat the different crystal orientations separately. Starting from the simple case of a PC with form isotropic elements (e.g. spheres), we explain how we treat the more complicated case of a PC with form anisotropic elements (e.g. cylinders).

The case of an opal is described in the Appendix A, as a typical example of the former type

of PCs. The calculation of reflectance and transmittance for different crystal orientations can easily be performed in this case since the discretization of form isotropic elements is the same whatever the crystal orientation is [Fig. 1(a)]. For instance, in the case of an opal, calculation for different orientations does not pose any particular issue because of the form isotropy of the single sphere present in the unit cell [6, 20, 21]. Indeed, isotropic elements such as spheres can be sliced into a set of coaxial cylinders with different radii for every crystal orientation [Fig. 1(b)].
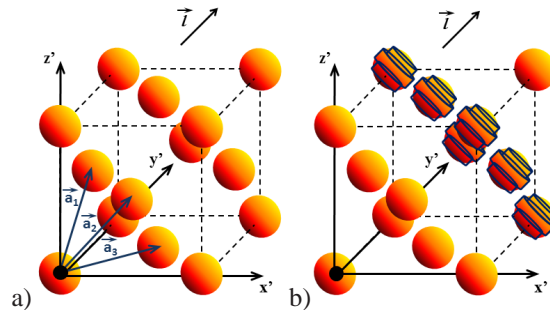

Fig. 1. a) Bravais lattice of an opal (face-centered cubic (FCC) photonic crystal) defined by primitive vectors $\vec{a}_1$, $\vec{a}_2$ and $\vec{a}_3$. b) In plane wave calculation methods such as RCWA, spheres are discretized into sets of cylinders with axes parallel to the crystal orientation $\vec{l}$ under study (e.g. here the (111) orientation). Whatever the crystal orientation $\vec{l}$ is, the discretization of spheres (form isotropic elements) is the same.

When the unit cell contains form anisotropic elements such as cylinders [Fig. 2], the discretization takes different forms according to the crystal orientation $\vec{l}$. Calculation of reflectance and transmittance according to different orientations is therefore more complicated to perform [Fig. 2], see also Appendix A for further details. For crystal orientations in Fig. 2(a-b), simple shapes can be used to describe elements and no special issue is encountered using RCWA. For the crystal orientation shown in Fig. 2(c), since Fourier transforms have to be calculated analytically using simple shapes, we are left with no choice but to slice the crystal into a multilayer medium with laterally homogenized layers. For this purpose, we developed a method allowing to calculate the reflectance for different crystal orientations with form anisotropic elements in the unit cell.

Our method relies on any standard thin film solver, based on e.g. the 1D SM formalism. The PC is approximated by an effective multilayer medium with laterally homogenized layers and whose composition must be defined for each crystal orientation under study [Fig. 3]. When light illuminates the crystal, the latter can be viewed (under certain assumptions discussed below) as a periodic stack of homogeneous layers whose refractive indices are calculated by spatial averaging [6, 22]. This homogenization procedure highly simplifies the resolution of Maxwell's equations, since the 3D problem is turned into a 1D problem.

Such an approximation is valid as far as the refractive index contrast between island and host materials is weak. The homogenization of layers results in translational invariance along any direction parallel to the layer surface, implying that no diffraction peaks except the Bragg peak occurs in the range of interest and reflection is therefore only specular. In order to neglect higher-order diffraction effects, islands must have a small-size compared to the wavelength, which is common in natural PCs [22,23] such as *Entimus imperialis* studied in section 3. Details on the Layer Homogenization (LH) method [Fig. 3] can be found in the Appendix B.

By averaging reflectance spectra calculated for different crystal orientations and incidence
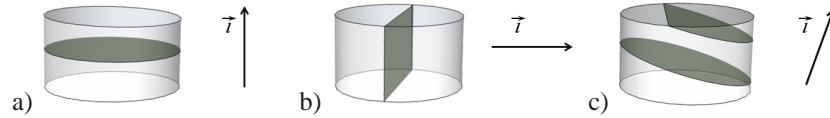
Fig. 2. In RCWA, elements composing the unit cell are discretized into a set of simple shapes: cylinders or parallelepipeds. Here is represented the case of a cylindrical element. a) Crystal orientation $\vec{l}$ parallel to the cylinder axis. b) Crystal orientation $\vec{l}$ perpendicular to the cylinder axis. c) Crystal orientation $\vec{l}$ neither parallel nor perpendicular to the axis. In this case, the discretization and the calculation of reflectance (transmittance) are more complicated to perform than in a or b.
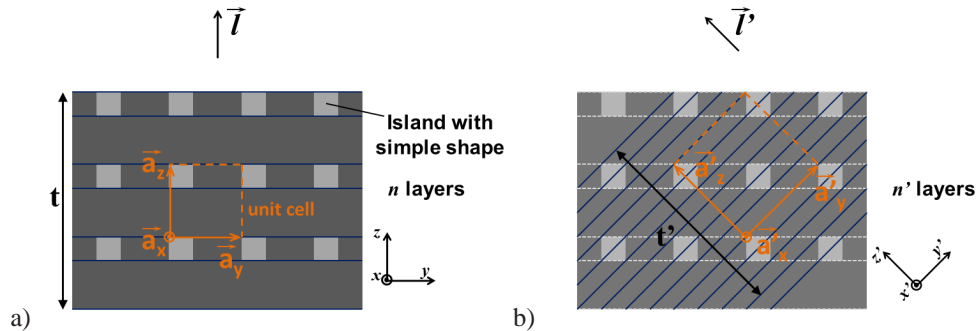

Fig. 3. a) The photonic crystal film is originally described for a specific crystal orientation $\vec{l}$, as a latteraly periodic stratified medium with n layers which may contain 2D lattices of cylindrical or parallelepipedic islands. The unit cell of the stratified medium is defined by $\vec{a}_x$, $\vec{a}_y$ and $\vec{a}_z$ translation vectors. $\vec{a}_z$ is the vector normal to the layer surfaces. The specific crystal orientation is parallel to $\vec{a}_z$. b) The new photonic crystal is described by another periodic stratified medium with n' layers and whose orientation $\vec{l}'$ is different from $\vec{a}_z$. The translation vectors $\vec{a}'_x$, $\vec{a}'_y$ and $\vec{a}'_z$ define the unit cell corresponding to this stratified medium. $\vec{a}'_z$ is parallel to $\vec{l}'$.

angles, the reflectance spectrum resulting from multiscale effects was simulated. Averaging is commonly used in order to simulate the photonic response of multiscale structures exhibiting diffusive properties due to, for instance, curved interfaces or large grains with different orientations in polycrystals [21, 22, 24].

3. Additive color effect in *Entimus imperialis*

Entimus imperialis is a Brazilian weevil displaying matt green spots on its elytra [Fig. 4(a)]. In spite of the fact that the perceived color is not iridescent, its origin is structural. The diamond beetle is indeed a nice example of additive photonic coloration due to a complex multi-length-scale structure, in this case a disordered set of ordered PC grains [9, 18]. The incident light is independently reflected by each crystal grain, producing single bright colors ranging from blue to orange [Fig. 4(b)] while the coloration observed at long distance is dull green [Fig. 4(a)]. The interaction of light with PC grains of different orientations alters the individual bright colorations leading to the loss of iridescence and a matt coloration perceived in the far-field.
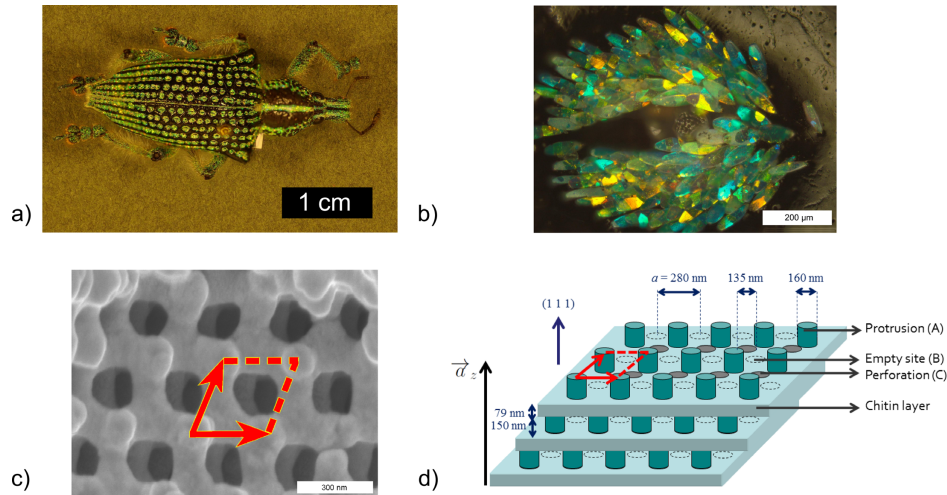
Fig. 4. a) *Entimus imperialis* displays matt green spots on its cuticle. b) Colorful scales covering the cuticle are at the origin of that coloration. The average length of scales is 100 μm, their width at half-length is 50 μm and their thickness is 2.20 μm c) SEM image of 3D photonic crystal grains (same photonic crystal with different orientations) found inside the scales. Translation vectors $\vec{a}_x$ and $\vec{a}_y$ of the photonic crystal unit cell are highlighted in red. d) The 3D photonic crystal structure is modeled by a stack of perforated chitin layers covered by a 2D lattice of cylindrical protrusions and corresponding to a FCC crystal.

3.1. Description of E. imperialis photonic structure

The cuticle of the weevil is covered by flat and elongated scales displaying bright colors and gathered inside millimeter size cavities on the cuticle surface [Fig. 4(b)]. These scales generally comprise a few photonic grains of about 2000 μm^2 exhibiting different colors. Inside the scales, a 3D PC nanostructure is found [Fig. 4(c)] and is modeled by thin chitin layers ($n_{chitin} = 1.56$ [25]) with a 2D lattice of cylindrical perforations ($n_{air} = 1$) and a 2D lattice of cylindrical protrusions made of chitin [Fig. 4(d)] [4, 9]. The unit cell therefore consists of one protrusion, one empty site (flat surface) and one perforation. Each PC grain gives rise to a bright color which depends on the crystal orientation and on the incidence angles. *Pachyrrynchus congestus pavonius*, a weevil from Philippines, presents a very similar photonic structure in its scales (producing an orange coloration) [22] but the PC grains are smaller (about 1500 μm^2). The average scale thickness is 2.20 μm ($\pm$ 0.25 μm). We note that the actual thickness has an influence on the reflectance spectrum. Following the same morphological analysis for identifying the stacking schemes as in [22], the photonic structure of *E. imperialis* was determined to be a FCC crystal with lattice parameter $d = \sqrt{2}a = 396$ nm [9]. The $(1\,1\,1)$ crystal orientation is perpendicular to the chitin layer surfaces. The model described here obviously consists of a periodic stratified medium with cylindrical islands. We note that the *E. imperialis* structure was identified to be a diamond crystal built from air cavities in other independant studies [11, 18, 26]. The lattice parameter was found to be 410 nm in [11] and 445 nm in [18, 26]. These values are relatively close to the lattice parameter we determined. The lattice model proposed in [11, 18, 26] has however a different symmetry (i.e. diamond). It contains no anisotropic elements and is therefore not an appropriate example for the problem discussed. Although our lattice model is different (FCC), similar additive color effects are found.

Despite the fact that the nanostructure consists of crystal grains from a single PC with different orientations, we first consider a grain with a unique orientation. Then, the disorder in

grain orientations is taken into account. We note here that a calculation method such as ray-tracing [27] is useless for studying such multiscale effects because there is no optical coupling between grains as a result of laying positions of the scales on the cuticle surface and of specular reflections.

3.2. Assessment of diffraction properties in the visible range

PCs by definition diffract light. However, higher-order diffraction peaks may appear in spectral range outside (below) the visible range. In this case, when only specular (Bragg) reflection remains in the visible range, higher-order diffraction has no effect on the perceived color. This is actually the case that is treated here.

We first assessed the diffraction properties of the photonic structure in the $(1\,1\,1)$ orientation, considering the periodicity in the planes parallel to the layer interfaces. For this purpose, we used the dominant reflected wavelength formula [6, 22] which was adapted in order to take diffraction into account. The dominant reflected wavelength formula is only valid within the limit of weak refractive index contrasts. When it is applied to 2D and 3D PCs [6,22], it predicts the position of the specular reflectance peaks:

$$\lambda = \frac{2p\sqrt{\bar{n}^2 - \sin^2\theta}}{m} \qquad (1)$$

where p is the distance between two parallel reticular planes corresponding to a given orientation, $\bar{n}$, the effective refractive index, θ the incidence angle and m is an integer. In this formula, 2D or 3D photonic crystals are approximated by homogenous effective media. For the $(1\,1\,1)$ orientation, the relation between the distance p and the lattice parameter d is $p = d\sqrt{3}/3 = 229\,\text{nm}$ [9]. p corresponds to the sum of the height of the protrusions and the thickness of the perforated chitin layer [Fig. 4(d)]. The effective refractive index $\bar{n}$ was evaluated to be equal to 1.23 [9]. When the incident light interacts with a laterally periodic medium, a reciprocal lattice vector $\vec{g}$ has to be added to the wavevector component $\vec{k}_{\parallel}$ that is parallel to the medium surface. Taking this into account, the dominant reflected wavelength formula at normal incidence ($\theta = 0°$) is [24]:

$$\lambda_g = \frac{2p\bar{n}}{\sqrt{m^2 + \left(\frac{pg}{\pi}\right)^2}}. \qquad (2)$$

The reflectance peaks due to diffraction are positioned at shorter wavelengths than the specular reflectance peak wavelength. For the six shortest non zero reciprocal $\vec{g}$-vectors (norm $\|\vec{g}\| = 4\pi/\sqrt{3}a$), diffraction peaks were located at 263 nm ($m = 1$) and 205 nm ($m = 2$), outside the visible range [9]. Higher diffraction orders, i.e. $\vec{g}$-vectors with higher norms, gave rise to reflectance peaks below 200 nm. The same procedure was applied to the $(1\,0\,0)$ orientation (with $p = d/2 = 198\,\text{nm}$) and showed that diffraction peaks were at 281 nm ($m = 1$) and 199 nm ($m = 2$), for the four shortest non zero $\vec{g}$-vectors ($\|\vec{g}\| = 2\pi/a$). From Eq. (2), we can therefore conclude that higher-order diffraction can be neglected in the visible range for the *E. imperialis* crystal in the $(1\,1\,1)$ and $(1\,0\,0)$ orientations, which justifies the use of the LH method.

Other orientations such as $(1\,1\,0)$, $(2\,0\,1)$, $(1\,2\,3)$, $(1\,2\,1)$ and $(2\,3\,3)$ were considered. Only the previously discused $(1\,1\,1)$ and $(1\,0\,0)$ orientations exhibit strong specular reflectance peaks in the visible range and higher-order diffraction out of this range. For the other directions, Bragg peaks were either present in the spectral range of interest but were relatively weak (less than 20%) and very narrow or were located at shorter wavelengths, out of the visible range.

Another way to assess the diffraction properties is using RCWA calculation which provides us with reflectance spectrum components corresponding to each recirpocal vector $\vec{g}$. The sum

of these components provides the total reflectance spectrum. The diffracted reflectance is defined as the difference between the total and the specular reflectances. The diffracted reflectance was found to be maximum at 225 nm and 204 nm and vanished to zero above 243 nm [Fig. 5], i.e. below the visible range [9]. The difference between the former value (225 nm) and the one calculated by Eq. (2) (263 nm) can be explained by the fact that the dominant reflected wavelength formula is valid at wavelengths larger than p. This RCWA calculation confirmed that only the specular order was reflected in the visible range. The LH method could therefore be used for predicting the reflectance of *E. imperialis*. These results agree with the highly directional reflectance of a single scale measured by scatterometry [18].
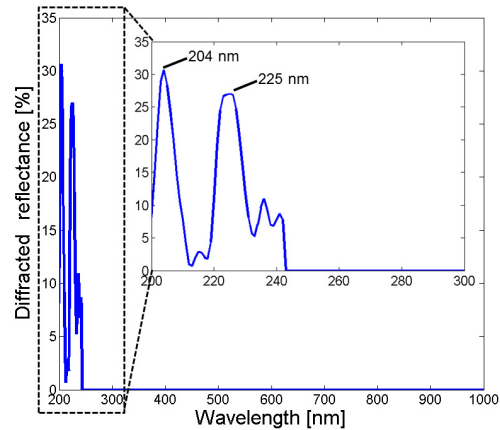

Fig. 5. Diffracted reflectance spectrum calculated by RCWA method. Diffraction occurs only below the visible part of the electromagnetic spectrum ($<$ 243 nm). Diffraction peaks are found at 225 nm and 204 nm.

3.3. *Reflectance spectra in the* $(1\,1\,1)$ *and* $(1\,0\,0)$ *orientations*

We used the LH method to compute the reflectance spectra in the $(1\,1\,1)$ and $(1\,0\,0)$ orientations for various incidence angles (Figs. 6 and 7). These orientations were the only ones to lead to significant spectral reflectance values in the visible range.

In the case of the $(1\,1\,1)$ crystal orientation, the first order Bragg reflectance peak was located around 577 nm at normal incidence [Fig. 6]. The related coloration was yellow. The dominant reflected wavelength at normal incidence was estimated to be 563 nm using $p = d\sqrt{3}/3 = 229$ nm [9]. Another reflectance peak was found at 297 nm. Eq. (1) showed that this peak corresponded to the $m = 2$ harmonics of Bragg reflection, i.e. $\lambda = 2 \times 229 \times 1.23/2 = 282$ nm. A blue shift of the reflectance spectrum with increasing incidence angle was observed as expected: the peak shifted from 577 nm (i.e. yellow) to 493 nm (i.e. blue) when the incidence angle θ varied from 0° to 45°.

For the $(1\,0\,0)$ orientation, the reflectance could be calculated using the LH method only because the PC film unit cell comprised form anisotropic elements (see section 2). The reflectance was found to be maximum around 530 nm (green color), at normal incidence [Fig. 7]. A value of 487 nm was obtained by using Eq. (1) with a distance between two reticular planes equal to $p = d/2 = 198$ nm. A shift of the peak position to 449 nm (violet) was observed when the incidence angle was increased to 45°.
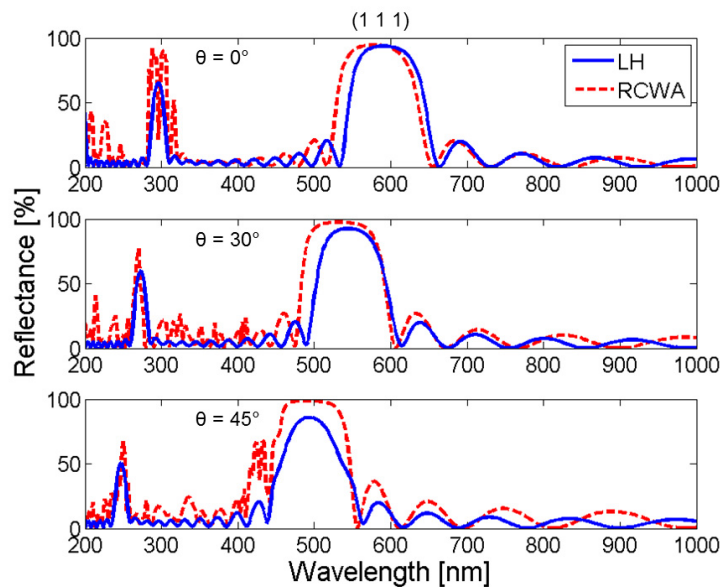
Fig. 6. Reflectance spectra in the (1 1 1) orientation calculated using two computational methods at different incidence angles θ. Curves labelled LH were simulated by the Layer Homogenization method and curves labelled RCWA were computed by RCWA method.
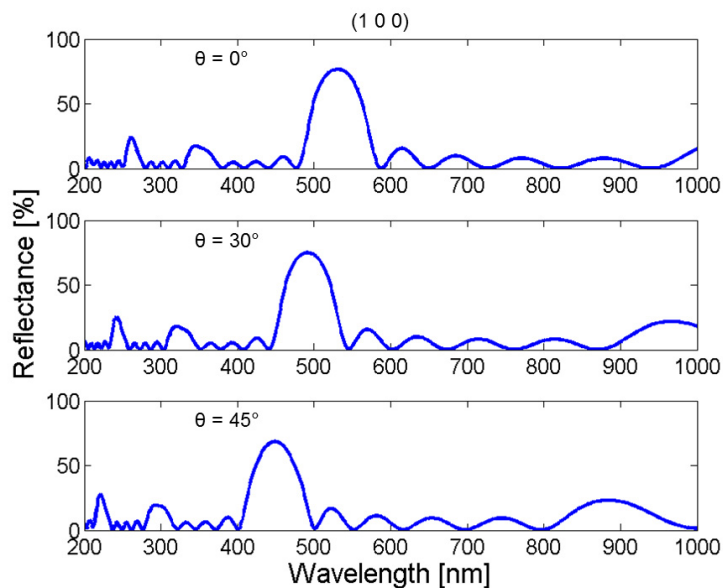

Fig. 7. Reflectance spectra in the (1 0 0) orientation calculated using the LH method at different incidence angles θ. A blue shift of the spectrum is observed when θ was increased.

3.4. Reflectance calculated by RCWA

For the sake of comparison, the reflectance spectrum in the $(1\,1\,1)$ orientation was simulated by RCWA. Indeed, for that specific orientation, the elements of the PC unit cell could be described by islands with simple shapes, i.e. cylinders in the present case. At normal incidence, the main peak was positioned around 578 nm and the calculated spectrum was very similar to the one predicted by our LH method [Fig. 6].

The increasing discrepancy between LH and RCWA at higher θ values is due to the increase of the parallel component of the incident wave vector $k_{\parallel} = k \sin \theta$. As θ increases, the apparent wavelength (i.e. in the plane parallel to the interfaces) decreases and therefore homogenization of the crystal structure in lateral directions is less and less justified.

The peak positions determined by the dominant reflected wavelength formula, Eq. (1), or deduced from the simulated reflectance spectra are all in good agreement (Table 1). At shorter wavelengths, the larger difference between LH method and dominant wavelength formula is explained by the fact that the calculation of the effective refractive index is only valid at long wavelengths.

Incidence angle	λ_{dom}	RCWA	LH
0°	563 nm [487 nm]	578 nm	590 nm [530 nm]
30°	514 nm [445 nm]	531 nm	544 nm [492 nm]
45°	460 nm [399 nm]	490 nm	494 nm [449 nm]

Table 1. Reflectance peak positions at various incidence angles (0°, 30° and 45°) for the $(1\,1\,1)$ orientation and $(1\,0\,0)$ orientation (between brackets) calculated using different methods are in good agreement. "λ_{dom}" and "LH" mean dominant wavelength formula and Layer Homogenization method, respectively. In the $(1\,0\,0)$ orientation, RCWA method cannot be used because the unit cell of the PC film comprises form anisotropic elements.

3.5. Multiscale averaging aspects

The different orientations of the grains give rise to a diversity of colorations. The resulting color was quantified using chromaticity coordinates, which were calculated from the reflectance spectrum and the source spectrum (assuming D_{65} illuminant). We used the 2-degree observer chromaticity diagram defined by the *Commission Internationale de l'Eclairage* (CIE) in 1931, following a method presented elsewhere [28]. Chromaticity coordinates corresponding to the $(1\,1\,1)$ and the $(1\,0\,0)$ orientations were calculated at various incidence angles (from 0° to 75° by step of 15°). They were found to be distributed in different parts of the chromaticity diagram (mainly in the yellow, green and blue parts) [Fig. 8]. Changes in the incidence angle and in the orientation of the grains give rise to yellow, green and blue colors, as observed in individual scales [Fig. 4]. However, the color perceived by human eye at long distance results from an additive color effect [9, 18]. The colorations produced by the different grain orientations are indeed "mixed" when observed in the far-field. When we calculate the chromaticity coordinates corresponding to the average of the simulated reflectance spectra, the related point is located in the green region [Fig. 8]. It corresponds to the color observed by the naked eye and measured experimentally in a previous study [9]. The additive coloration of the cuticle of *E. imperialis* is therefore produced by a mix of a variety of colors due to two specific orientations of the PC present in the polycrystal nanostructure of the weevil. Other examples of additive photonic colors due to a spatial averaging of colors produced by different orientations of one single FCC 3D crystal are found in nature: on the cuticle of weevils such as *Pachyrrhynchus congestus pavonius* [22], *Pachyrhynchus argus* [23] and *Eupholus magnificus* [29], on longhorn beetles such as *Prosopocera lactator* [20] and *Pseudomyagrus waterhousei* [21] or on butterfly wings

like *Cyanophrys remus* [30]. The difference between the case of the diamond weevil and the other ones is that the crystal grains in *E. imperialis* are very regular and their size is much greater than in the other cases.
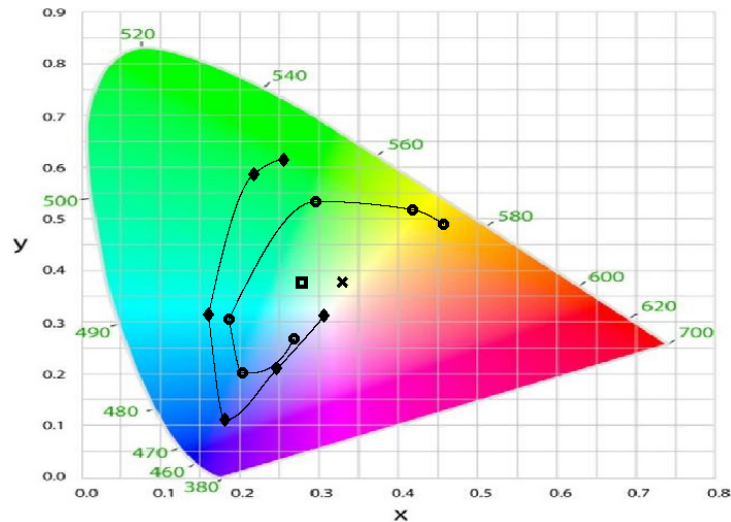

Fig. 8. Chromaticity coordinates calculated for the $(1\,0\,0)$ orientation ($\blacklozenge$) and for the $(1\,1\,1)$ orientation ($\bigcirc$) at various incidence angles (from $0°$ to $75°$ by step of $15°$). The colors produced by the interaction of light with the photonic polycrystal are various. The coordinates calculated from the average of the reflectance spectra ($\square$) fall into the green area of the diagram. Chromaticity coordinates from far-field reflectance [9] are represented by a cross ($\times$).

4. Conclusion

We investigated additive photonic colors arised in polycrystals due to grains of a single photonic crystal. The computation of the reflectance or transmittance for different crystal orientations turned out to be cumbersome to perform because the crystal unit cell contained form anisotropic elements. To solve this issue, we developed an original method based on homogenization of layers. Thanks to this homogenization, the reflectance spectra could be calculated using a standard thin film solver, which reduced considerably the computation time. The method assumed that there are no diffraction peaks except Bragg peak in the spectral range of interest (i.e. visible). The additive color effect was taken into account by averaging reflectance spectra calculated for various crystal orientations and incidence angles. The usefulness of our method was demonstrated in the case of *Entimus imperialis* weevil, which satisfied all required conditions to apply the method.

Appendix A: RCWA method and form anisotropic elements

The RCWA method relies on a 3D scattering matrix (3D SM) electromagnetic formalism [5,6]. It exactly solves Maxwell's equations for inhomogeneous optical media which are stratified and laterally periodic. In this method, a 3D PC is therefore viewed as (and sometimes approximated by) a stratified medium. The unit cell, defined by translation vectors $\overrightarrow{a}_x$, $\overrightarrow{a}_y$ and $\overrightarrow{a}_z$, is formed by an arbitrary pattern of (non overlapping) islands of various materials (e.g. air voids) embedded in a host and is repeated periodically in the lateral directions. Each layer of the stratified

medium is assumed to be homogeneous along the vertical direction.

A PC is described by its Bravais lattice which is generated by linear combinations of primitive vectors $\vec{a}_1$, $\vec{a}_2$ and $\vec{a}_3$ [Fig. 1(a)]. These three vectors define the so-called crystal unit cell. In the framework of RCWA, a 3D PC film is treated as a stratified medium between the incidence medium and the substrate (homogeneous media, characterized by dielectric constants ε_i and ε_s). The PC film is therefore defined by layers perpendicular to the crystal orientation $\vec{l}$ under study. Any element composing the crystal unit cell is approximated by a set of islands with simple shapes (cylinders or parallelepipeds). For instance, a sphere is discretized into a stack of coaxial cylinders with different radii [Fig. 1(b)].

In the case of a PC with form anisotropic elements such as cylinders, for instance, three situations can be distinguished. First, when the crystal orientation $\vec{l}$ under which the PC is viewed is parallel to the cylinder axis [Fig. 2(a)], the cylinder is divided into a set of cylindrical islands and the reflectance for that orientation is calculated just as in the case of isotropic elements. Second, when the crystal orientation $\vec{l}$ is perpendicular to the cylinder axis, islands consist of rectangular parallelepipeds [Fig. 2(b)]. Again the reflectance is calculated as for isotropic elements. Third, when the crystal orientation $\vec{l}$ is neither parallel nor perpendicular to the cylinder axis, islands consist of prisms with ellipse and truncated ellipse basis [Fig. 2(c)]. These islands can hardly be approximated by cylinders or parallelepipeds.

Appendix B: Layer Homogenization method

Let us consider a crystal orientation $\vec{l}$ in which the PC film can be assimilated to a latterally periodic stratified medium with islands of simple shapes such as cylinders for instance [Fig. 3]. Let us define $\{xyz\}$, the cartesian coordinate basis of that original description of the PC film [Fig. 3(a)], with the z axis perpendicular to the layer planes ($\vec{l}$ parallel to z direction). In this basis, we define the translation vectors ($\vec{a}_x$ and $\vec{a}_y$) of the 2D lattice in lateral directions [Fig. 3(a)]. The translation vector $\vec{a}_z$, normal to the layer planes is therefore aligned with the specific crystal orientation $\vec{l}$ we selected originally. Let us then map the values of the dielectric constant ε_{ijk} in the unit cell of each original layer by defining N^3 grid points $\vec{r}_{ijk}$. The grid positions are then expressed in a new basis $\{x'y'z'\}$ which will be introduced hereafter: $\vec{r}'_{ijk} = A\vec{r}_{ijk}$, where A is the coordinate transformation matrix. The original description of the PC film requires n layers of thickness d_j such then $\sum_{j=1}^{n} d_j = t$, where t is the thickness of the film.

Let us then consider another crystal orientation $\vec{l}'$ in which the PC film can no more be assimilated to a stratified medium with simple shape islands [Fig. 3]. For that specific orientation, the new description of the film is made using a stratified medium of n' homogeneous layers with the identical thickness d'. The $\{x'y'z'\}$ basis is the basis associated with the new homogenized description of the PC film. A unit cell corresponding to the new description must be defined in order to perform the spatial averaging of ε which is required for homogenization. Let us define $\vec{a}'_x$, $\vec{a}'_y$ and $\vec{a}'_z$ the translation vectors of this new unit cell with $\vec{a}'_z$ aligned in the new crystal orientation $\vec{l}'$ [Fig. 3(b)]. The periodicity along the orientation $\vec{l}'$ perpendicular to the new layers is determined by defining $\vec{a}'_z$ as the linear combination of the primitive vectors $\vec{a}_1$, $\vec{a}_2$ and $\vec{a}_3$ of the PC unit cell having the smallest norm. The new lateral translation vectors $\vec{a}'_x$ and $\vec{a}'_y$ are defined by the linear combinations of $\vec{a}_1$, $\vec{a}_2$ and $\vec{a}_3$ falling the new layer plane (i.e. perpendicular to $\vec{l}'$) which give rise to the smallest 2D unit cell. Using the mapping of the dielectric constant in the new basis, the effective (homogeneous) values of the dielectric constants $\bar{\varepsilon}_k$ in each new layer k are calculated by spatial averaging over the new unit cell.

Whereas the original description of the PC film defines the film thickness as t, the total

thickness $t' = n' \times d'$ of the film in the new description has to be arbitrarily set. It was chosen as the integer multiple of $\left\|\overrightarrow{d'_z}\right\|$ which was the closest to t. Having determined the periodicity and effective dielectric constants $\overline{\varepsilon}_k$ of the new layers, the new description of the PC film as a homogeneous stratified medium is now completed. Reflectance is eventually calculated by using a standard thin film solver. Of course, convergence must be checked according to the number of grid points N^3 and the layer thickness d' (see Appendix C).

Appendix C: Convergence aspects

Convergence studies were performed according to the number of grid points N^3 and the thickness of homogenized layers d'. In the case of *E. imperialis*, $N^3 = 25^3$ grid points were needed and d' had to be equal to 25 nm in order to achieve numerical convergence. The computations were performed on an High Performance Computing (HPC) cluster consisting of 85 compute nodes for a peak performance of 9 teraflops, 6 interactive nodes and file servers with about 45 TB of disk space available. CPU computation times for the $(1\,0\,0)$ and the $(1\,1\,1)$ orientations were shorter than 120 and 100 minutes (more than 99% for grid computation), respectively, and the maximum used memories were below 800 MB and 3 GB, respectively.

Regarding RCWA calculation, the convergence was checked according to the number of plane waves. The minimum number of plane waves which was needed for achieving numerical convergence was found to be equal to 7×7. Computation time was 220 minutes for the $(1\,1\,1)$ orientation.

Acknowledgments